

N-terminal modification of VEGF-A C-terminus derived peptides delineates structural features involved in neuropilin-1 binding and functional activity.

Haiyan Jia ^{[a],#}, Rehan Aqil ^{[b],#}, Lili Cheng ^[a], Chris Chapman ^[b], Shaheda Shaikh ^[b], Ashley Jarvis ^[b], AW Edith Chan ^[d], Basil Hartzoulakis ^{[b],†}, Ian M Evans ^[a], Antonina Frolov ^[a], Prof. John Martin ^[a], Paul Frankel ^[a], Snezana Djordevic ^[c], Prof. Ian C Zachary ^[a], and Prof. David L Selwood ^{[d],*}

Contact: d.selwood@ucl.ac.uk

^[a]UK Centre for Cardiovascular Biology and Medicine, Division of Medicine, University College London, London WC1E 6JJ, UK.

^[b]NCE Discovery (Domainex Ltd), 162 Cambridge Science Park, Cambridge CB4 0GH, UK.

^[c]Institute of Structural and Molecular Biology, University College London, London, UK.

^[d]Wolfson Institute for Biomedical Research, UCL, Gower Street, London WC1E 6BT, UK.

#these authors contributed equally to this work.

†Current address: Chemiverse Ltd., Cambridge, UK

*Corresponding author Email: Prof. David Selwood (d.selwood@ucl.ac.uk).

Abstract

The interaction between VEGF-A and its neuropilin (NRP) receptors mediates a number of important biological effects. NRP1 and the related molecule NRP2 are widely-expressed on multiple tumour types and throughout the tumour vasculature, and are emerging as critical molecules required for the progression of angiogenic diseases. Given the increasing evidence supporting a role for NRP1 in tumour development, there is growing interest in developing inhibitors of NRP1 interactions with VEGF and its other ligands. In order to probe the interaction we synthesized a number of exon 7 and 8-derived bicyclic peptides with N-terminal lipophilic groups and found a simple N-octanoyl derivative (EG00086) to be the most potent and functionally active. Detailed modeling studies indicated that new intramolecular hydrogen bonds were formed stabilizing the structure and possibly contributing to the potency. Removal of a salt bridge between D142 and R164 implicated in VEGF-A binding to neuropilin-1 had a minor effect on potency. Isothermal calorimetry was used to assess binding of EG00086 to NRP1 & NRP2 and the stability of the peptide in serum and in vivo was investigated. EG00086 is a potent blocker of VEGF promoted cellular adhesion to extracellular matrices and phosphorylation of p130Cas contributes to this effect.

Short title: N-terminal modification of VEGF-A C-terminus derived peptides

Keywords: VEGF-A, neuropilin, cancer, cell adhesion, p130Cas, melanoma, bicyclic peptide.

Introduction

Neuropilin-1 (NRP1) is a cell-surface receptor capable of augmenting or changing the activity of several growth factors including several isoforms of VEGF, PLGF, HGF (scatter factor) and TGF- β . It is recognized that NRP1 itself can signal through a number of partly defined mechanisms including signaling through an intracellular PDZ binding domain and also via internalization of the NRP1 receptor.^[1-3] In structural terms NRP-1 is a transmembrane glycoprotein containing a large multimodular extracellular region, a transmembrane helix and a small intracellular domain.^[4-6] NRP1 is essential for vascular and neuronal development^[7-8] and these two roles are thought to be mediated by semaphorin (Sema) and Vascular Endothelial Growth Factor ligands for NRP1 in sensory neurons and endothelial cells, respectively.^[9-12] The major VEGF-A ligand binding site on NRP1 is in the extracellular b1 domain with a contribution of the b2 domain, whereas recognition of Sema3A is mediated by the a1/a2 and b1/b2 domains.^[12] NRP1 is also thought to augment VEGF-A signalling through its VEGFR2 receptor.^[11]

NRP1 and the related protein NRP2 are widely expressed on multiple tumor types and on the tumour vasculature, and play a role in tumour cell signaling and cell migration stimulated by several growth factors including PDGF, HGF and TGF- β .^[13-15] Our recent work has identified a key role for NRP1 in mediating growth factor stimulation of tyrosine phosphorylation of p130Cas, an adapter molecule with a central role in both migration and invasion of cancer cells.^[16-17] ^[18] ^[17-19] The involvement of a p130Cas complex situated at focal adhesions may drive the release of matrix metallo-proteases, such as MT1-MMP that then serve to degrade the matrix and facilitate cell migration.^[20] Recently the snake venom component rhodocetin- $\alpha\beta$ has been shown promote endothelial cell motility. Rhodocetin- $\alpha\beta$ binds NRP1 and induces complex formation with c-Met. This leads to paxillin phosphorylation and redistribution at focal adhesions.^[21] Thus a number of mechanisms controlling motility and adhesion have been shown to operate via neuropilin.

Furthermore, NRP1 and NRP2 are implicated in several aspects of tumour pathogenesis. Anti-NRP1 antibodies can reduce in vivo tumour growth^[22] whereas NRP2 antibodies can block metastasis operating through the lymphatic system and a VEGFR-3/NRP2 axis.^[23] NRP1 may contribute to the generation of cancer stem cells in squamous skin cancer and glioma.^[24-25] NRP1 is also expressed in subsets of CD4⁺ regulatory T cells (Tregs)^[26] and a role of NRP1 in mediating tumour T-reg infiltration and suppression of T-cell immunity in some experimental tumour models has recently been described. Treg-specific ablation of Nrp1 results in an increased CD8⁺ T-cell response and impaired melanoma tumour growth.^[27]

With the increasing evidence supporting a role for NRP1 in tumour development, there has been growing interest in developing inhibitors of NRP1 interactions with VEGF-A and its other ligands. These include anti-NRP1 antibodies,^[22] bicyclic peptides mimicking the C-terminus of VEGF-A,^[28] linear peptides such as ATWLPPR,^[29] C-end rule (or CendR) peptides.^[30] and a recently described cyclic peptide/mini-protein based on the kalata cyclotide scaffold.^[31] This latter peptide is unusual in that it does not contain a C-terminal arginine present in other peptidic antagonists of VEGF-A binding to NRP1; in this case the arginine is incorporated in a ring. The Genentech NRP1 antibodies, are distinct in that a C-terminal histidine is observed to bind into the arginine pocket.^[32] A small molecule antagonist of the NRP1 VEGF-A interaction, EG00229, has also been developed.^[33]

Several peptides have been developed as therapeutics, including enfuvirtide (T-20), a 36 amino acid linear peptide licensed for the treatment of HIV infection.^[34] Orally-active examples of peptide therapeutics include the immuno-suppressive cyclic peptide cyclosporin-A, which shows up to 65% oral bioavailability in micro-suspension formulations.^[35] Peptides can additionally be linked to antibodies to provide improved pharmacokinetics.^[36]

We previously reported a bicyclic disulfide linked peptide (**1**, EG3287, Table 1) derived from the C-terminal 28 amino acid residues of VEGF-A encoded by exon 8 and the C-terminal portion of VEGF-A exon 7, and found it to have a defined structure in solution as determined by NMR, similar to the structure of the native VEGF-A₁₆₅ C-terminal domain.^[28] EG3287 is a selective inhibitor of VEGF-A binding to NRP1 and inhibits biological activities of VEGF-A in endothelial cells.^[28, 37-38] N-terminal modification has been shown to improve activity of a variety of peptides, either through enhancement of proteolytic stability^[39] or by increasing potency.^[40] We made a series of N-terminal modified EG3287 analogues with systematic changes designed to explore key binding residues and the effect of truncation of the C-terminal exon 8-derived region on ligand binding and in functional assays. From these studies we identified a peptide, **2**, EG00086 with improved potency and functional activity. Isothermal calorimetry was used to assess binding of EG00086 to NRP1 and NRP2 and the stability of the peptide in serum and in vivo was investigated. Our data demonstrate that an N-octanoyl derivative, EG00086, is a potent blocker of VEGF-A binding to NRP1 and exhibits functional effects in endothelial and tumour cells in culture.

PLACE TABLE 1 NEAR THIS PARAGRAPH

Materials and Methods

Synthesis of bicyclic peptides

Standard Fmoc based peptide chemistry was utilised in the synthesis of the bicyclic peptides as described.^[28] Detailed chemistry procedures are provided in the supplementary data.

Molecular modelling and dynamics:

All protein modelling and dynamics described in this work were carried using MOE (Molecular Operating Environment) package (version 2011.10). The PDB structure 4deq (Neuropilin-1/VEGF-A, human) was used as the initial protein template. This PDB file contained 2 chains. Chain A VEGF-A heparin domain is fully engaged the NRP1-b1 domain of chain B. The coordinates of part of the C-terminus of chain A (-

SCKNTDSRCKARQLELNERTCRCDKPRR-OH) was used to model our peptide EG00086, C₇H₁₅-(C=O)-SCKNTDSRCKARQLELNERTCRCDKPRR-OH. The N-terminal chain (C₇H₁₅-(C=O)-) was built in MOE using the “Molecular Builder”. This N-terminal chain (C₇H₁₅-(C=O)-) was set in an extended conformation. The model peptide was merged into a PDB file by aligning to chain A from 4deq. The initial model used for the dynamics study thus contained only chain B of 4deq and our modelled peptide, EG00086.

“Structure Preparation” in MOE was used to prepare the above model peptide for dynamics simulation. This procedure included adding hydrogens to and protonating the protein/peptide chains and sidechains. All molecular dynamics simulations were conducted in vacuo using “Simulations-Dynamics” in MOE. The protocol used for the dynamics simulations is as follows: algorithm - Nosé-Poincaré-Andersen Hamiltonian equations of motion (NPA); temperature – constant at 300 °K; mode – equilibration for 100 ps, forcefield – CHARMM22, cutoff at 8Å. Conformations were collected in trajectory files every 0.5 ps, providing 200 peptide/protein conformers for each run.

Data analysis was carried out also in MOE using the graphics interface. The conformers were already aligned in MOE and were examined manually.

Purification of NRP1b1 and NRP2b1

Gene sequences corresponding to the residues of the b1 domains were cloned into pET15b vectors and expressed in Rosetta-gami 2 (DE3) pLysS cells (EMD, #71403-3) as previously described.^[41] Several milligrams of NRP1b1 and NRP2b1 were prepared using a standard protocol that includes Ni²⁺- affinity purification, removal of the hexahistidine tag by TEV protease, size exclusion chromatography (Superdex 75) and ion exchange chromatography on SP FF Sepharose column.^[33] ITC measurements were carried out with the freshly prepared proteins.

ITC experimental details:

Isothermal titration calorimetry experiments were carried out in a reaction buffer (20 mM Tris pH 7.9, 50 mM NaCl) using a VP-ITC titration calorimeter (*MicroCal, LLC*) with a reaction cell volume of 1.4 ml at 21 °C. Before running binding experiments, NRP1b1 and NRP2b1 samples were each dialyzed in the same buffer and all solutions, including the buffer that was used for heat dilution measurements, were degassed and filtered just before loading into the calorimeter. 10 μM NRP2b1 or 5 μM NRP1b1 in the reaction cell was titrated with the 100 μM stock solutions of EG00086 (or 50 μM compound for NRP1b1 titrations). 19 consecutive injections of 15 μL at 2 second/μL were applied at 4 minutes intervals, while stirring the reaction solution at 300 rpm constant speed. For heat of dilution measurements, 1.4 mL of reaction buffer in the reaction cell was titrated by 300 μL of 100 μM (or 50 μM) peptide and this value was subtracted from the measured heats of binding. Protein concentrations of the samples used in these experiments were estimated by UV absorbance measurements at 280nm.

Cell culture

Porcine aortic endothelial cells expressing NRP1 (PAE/NRP1) were provided by Dr. Shay Soker. The cells were grown in Ham's F12 medium containing 10% FBS and 25 µg/mL hygromycin B. PAE cells expressing VEGFR-2 (PAE/VEGFR-2) were provided by Professor Lena Claesson-Welsh and grown in Ham's F12 medium containing 10% FBS and 250 µg/mL gentamicin G418. Human tumour cell lines lung A549 and kidney ACHN, originally from ECACC, were provided by Quintiles Limited (Edinburgh, UK) and grown in RPMI 1640 medium/L-glutamine (Invitrogen, Paisley, UK) containing 10% FBS. Human umbilical vein endothelial cells (HUVECs) were purchased from TCS CellWorks (Buckingham, UK) and cultured in endothelial basal medium, (EBM; Cambrex BioScience Ltd, Nottingham, UK) supplemented with gentamycin-ampicillin, epidermal growth factor and bovine brain extract (Singlequots; Cambrex) and 10% FCS. HUVECs used in experiments were no more than passage 6.

¹²⁵I-VEGF binding

Binding displacement experiments were performed in cells grown to confluence in 24-well plates as described previously,^[28] using the indicated concentrations of peptides and 0.1 nM ¹²⁵I-VEGF (1200-1800 Ci/mmol, GE Healthcare, Little Chalfont, UK). Non-specific binding was determined in the presence of 100-fold excess unlabelled VEGF (R & D Systems, Abingdon, UK).

Binding kinetics

Surface plasmon resonance (SPR) measurements of binding kinetics of EG00086 or VEGF with NRP1 were performed on a BIAcore T200 instrument (GE Healthcare, Little Chalfont, UK) at 25°C. Recombinant NRP1 (R & D Systems, Abingdon, UK) was immobilized onto a CM5 sensor chip by amine coupling chemistry according to the manufacturer's instructions. Kinetic experiments were set up using the multi-cycle mode. The EG00086 or VEGF samples in running buffer (PBS, pH 7.4, 0.005% surfactant P20) were injected sequentially at increasing concentration over both the NRP1-coated and the reference (non-coated) surfaces at a flow rate of 30 µl/min. After each run, the sensor chip was regenerated by injection of 50 mM aq. HCl. The binding sensorgrams were double referenced prior to global fitting of the concentration series. Association and dissociation rates (k_a and k_d) were obtained by fitting the sensorgrams with the 1:1 Langmuir binding model using the BIAevaluation T200 software (version 1.0). Equilibrium affinity constant (K_D) was derived from the kinetic parameters ($K_D=k_d/k_a$).

Cell viability

Cell viability was determined by measurement of conversion of the tetrazolium salt XTT to form formazan dye. Tumour cells were seeded at a density of 4×10^3 cells per well of 96-well plates in 100 µL serum-free medium containing the indicated concentrations of 5-FU or paclitaxel in the absence or presence of EG00086 at 10 µM. After 44 h incubation, XTT labelling reagent mixture (Roche Diagnostics, East Sussex, UK) was added to the cultures and they were incubated for a further 4 h. The formazan product was then measured at $A_{490 \text{ nm}}$ with a reference wavelength at 595 nm.

Cell-matrix adhesion

Cell adhesion to extracellular matrix (ECM) proteins including basement membrane protein complex (BMC), laminin I, collagen IV, fibronectin or vitronectin was measured by the Innocyte ECM cell adhesion assay (Calbiochem Inc, Nottingham, UK). Cells were detached with a non-enzyme cell dissociation solution, washed, and resuspended in RPMI 1640 medium. Cells were pre-treated with EG00086 or EG3287 at the indicated concentrations for 30 min and then seeded at a density of 3×10^4 cells per matrix-coated well in 96-well plates. After 1.5 h of incubation, cells were washed with PBS. The attached cells were labelled with the green fluorescent dye calcein-AM and measured using a fluorescence plate reader at an excitation wavelength of 485 nm and an emission wavelength of 510 nm.

Immunoblotting

For immunoblotting, cells were lysed in a solution containing 50 mM Tris-HCl (pH 7.5), 1% Triton X-100, 150 mM NaCl, 5 mM EDTA, complete protease inhibitor (Roche) and phosphatase inhibitors I & II (Sigma) and analysed by SDS-PAGE using 4-12% Bis-Tris gels; (Nupage; Invitrogen) followed by electrotransfer onto Invitrolon PVDF membranes (Invitrogen). Membranes were blocked with 5% w/v non-fat dry milk and 0.1% v/v Tween-20 in tris-buffered saline (TBS-T), for 1 h at room temperature, before being probed with the primary antibody by overnight incubation at 4°C, followed by incubation for 1 h at room temperature with a horseradish peroxidase-linked secondary antibody (Santa-Cruz) and detection using ECL plus reagents (GE Healthcare, Little Chalfont, UK), following the manufacturer's protocol. Immunoblots were quantified by scanning films with a calibration strip and analysed by densitometry using Image J (US National Institutes of Health; <http://rsb.info.nih.gov/ij/>).

Statistical analysis

Data were analysed using Prism (version 4.0) statistical packages. Comparisons of two sets of variables were performed using the Student's *t* test or *t* test with Welch's correction where appropriate. Differences among three concentrations of peptides were evaluated using the one-way analysis of variance (ANOVA) with Bonferroni's multiple comparison tests. Differences between two treatment groups at various concentrations were analysed using the two-way ANOVA with Bonferroni's post-tests. Values represent means \pm SEM determined from the results of three independent experiments each performed in duplicates or triplicates unless where stated. A value of $p < 0.05$ was considered statistically significant.

Results and Discussion

Design and synthesis of N-capped exon 7/8 analogues.

We hypothesized that N-terminal modifications to the peptide EG3287 could have an effect on the conformational stability of the peptide, or afford access to alternative binding regions of the NRP1b1 domain to increase potency. We selected a set of broadly lipophilic N-capping carboxylic acids to test this hypothesis ranging from simple biphenyl or naphthyl groups to aliphatic chains. We also tested the effect of alanine substitution in the exon 8

encoded region as an R to A substitution was noted to improve potency in a simple set of exon 8-mimicking linear peptides.^[33] A C-terminal arginine truncated analogue was also synthesized to investigate the effect of proteolytic cleavage of the C-terminal arginine.

The synthesis of our target peptides was accomplished using standard Fmoc solid phase methodology and cleavage of the linear peptide from the resin. The linear peptide was then subjected to sequential orthogonal disulfide bond formation using potassium ferricyanide ($K_3Fe(CN)_6$) for the first cyclisation and iodine for the cysteine, acetamidomethyl deprotection and second disulfide bond formation (Scheme 1). This methodology produces the disulfide bonded peptides in a defined disulfide bond geometry corresponding to the naturally observed and most active stereo-isomer.^[28] In order to introduce the N-terminal acetylation (N-capping) the peptides were acetylated using HOBt, DIC, DMF coupling conditions with the appropriate carboxylic acid while still attached to the solid phase. Amino acid substitutions (X in Scheme 1) or truncations in the exon 8 encoded region (CDKPRR) were introduced early in the solid phase synthesis and did not adversely affect the synthesis and isolation procedures.

Binding of modified peptides to NRP1 expressing PAE cells.

Binding of the peptides was assessed in an assay of specific, high-affinity ^{125}I -VEGF- A_{165} binding to porcine aortic endothelial cells (PAE) expressing NRP1 in the absence of other VEGF-A receptors^[28] (see Table 1). The binding activity was highly sensitive to the N-acylated structure with larger aryl acyl groups being disfavored and generally having much less activity than the underivatized EG3287. Notably peptide **2**, EG00086 (N-octanoyl) and peptide **3**, (N-acetyl-2-naphthoyl capped) had IC_{50} s for inhibition of ^{125}I -VEGF- A_{165} binding respectively four fold and two fold lower than that of EG3287, indicating increased potency. In contrast, the 7-hydroxynaphthylacetic acid, **4** and the larger aryl acid capped peptides **5** and **6** showed poor binding. R to A substitution of the amino acid in the exon 8 encoded region (CDKPRR) decreased the binding activity of EG00086 (peptide **7**) and of **3** (peptide **8**) (approximately two fold decrease in IC_{50}). Although this amino acid change increases the potency of shorter linear peptides^[33] a significant change in the structure of the C-terminus of VEGF-A has been noted where a salt bridge is formed between residues D142 and R163.^[42] Removal of this bridge may prevent formation of an optimal binding conformation. Two C-terminal arginine truncated peptides **9** (arginine truncated EG3287) and **10** (arginine truncated EG00086) showed reduced, but still significant, activity in the binding assay, indicating that possible proteolysis would not inactivate these peptides. The N-terminal modification in EG00086 maintained the specificity for NRP1 over VEGFR2, as evidenced by the lack of any effect on binding of VEGF-A to PAE cells expressing VEGFR2 (Figure 1, A & B).

Characterization of the EG00086-NRP1 interaction using surface plasmon resonance (SPR).

Real-time SPR analysis was carried out to characterise the binding kinetics for EG00086 to immobilized NRP1 extracellular domain. The natural ligand VEGF-A was first tested for binding to immobilized NRP1. Global fitting of the resulting sensorgram in Figure 1C to the parameters yielded a k_a of $7.6 \times 10^9 M^{-1} s^{-1}$, a k_d of $4.7 \times 10^1 s^{-1}$ and a derived K_D of 6 nM.

The kinetic parameters for the binding of EG00086 to NRP1 were a k_a of $3.9 \times 10^5 \text{ M}^{-1} \text{ s}^{-1}$, a k_d of $2.9 \times 10^{-2} \text{ s}^{-1}$ and a derived K_D of 76 nM (Figure 1C). Both on and off rate constants for EG00086 were much slower than those for VEGF-A though the on rates were most affected. The potency of EG00086 for immobilised recombinant NRP1 extracellular domain was significantly higher than that indicated by cellular binding assays (Figure 1A).

Assessment of the thermodynamics of EG00086 binding to NRP1 and NRP2 using isothermal titration calorimetry (ITC).

We next used ITC to determine the binding thermodynamics for EG00086. In addition, this technique allowed us to assess the binding of our peptides to NRP2. We utilised purified recombinant NRP1 b1 and NRP2 b1 domains for these experiments. EG00086 binds to NRP1 b1 and NRP2 b1 domains with affinities in the μM range, though the EG00086 affinity for NRP2 is 3 to 4 fold weaker than for NRP1 (Figure 2 A,B). These studies showed that EG00086 binding to NRP1 b1 domain is dominated by enthalpic contributions, presumably through a network of H-bonds and ion-pair interactions as observed in the crystal structures of NRP1 binding molecules such as EG00229 and tuftsin.^[33, 43] In contrast, entropic contributions were minimal (Table 2). This data does not point to a major hydrophobic interaction being formed between EG00086 and NRP1 or NRP2. While the affinity constants determined by ITC were in agreement with data from the cell-based binding assays they were significantly higher than that obtained by SPR analysis. The discrepancy might be the result of the SPR analysis involving an immobilised form of neuropilin-1 containing a1a2b1b2 domains while the ITC analysis was carried out on an isolated b1 domain. In addition to the possible consequences of the immobilisation process^[44] it was previously reported that affinity of VEGF for neuropilin is influenced by density of NRP1 on a sensor chip^[45] raising the possibility that some type of cooperativity for ligand binding might be observed under these conditions. The difference between NRP2 and NRP1 in their apparent affinity for EG00086 may be due to the change in the binding site caused by a single residue insertion in the loop 1 of the NRP2 ligand binding region. This possibility is explored in the following section using molecular modelling.

Molecular dynamics (MD) and modeling

Modeling of peptides and protein complexes. In the X-ray co-crystal structure of human NRP1/VEGF-A fusion protein, PDB 4deq,^[42] the VEGF-A heparin binding domain engages completely with the NRP1 b1 domain. The coordinates corresponding to the amino acid sequence (SCKNTDSRCKARQLELNERTCRCDKPRR) of our two peptides, EG00086 and EG3287, were taken from the VEGF-A structure in this PDB entry and were used as the initial conformations of the two peptides. For EG3287, the N-terminus was not capped (i.e. free NH_2); for EG00086, the N-terminus, $\text{C}_7\text{H}_{15}\text{-(C=O)-}^*$ was built in MOE ^[46], adopting a linear alkyl chain conformation. We used the conformation based on the structure of the bound C-terminus of VEGF-A^[42] rather than the more open structure observed for the intact exon-7 and 8 fragment of VEGF-A or the EG3287 peptide. The coordinates for NRP1 b1 were the same as the B chain from 4deq. A model for each peptide complexed to NRP1 b1 was formed. The initial coordinates for NRP2 b1 were from PDB file 2qqj and were superposed

onto 4deq using structural alignment and superpose techniques in MOE. The two isoforms overlay quite well. EG00086 was then added to form a model of the complex with NRP2 b1.

EG00086 binding to b1 domain of NRP1 and NRP2. In our model, EG00086 binds in a similar way to VEGF-A binding in the X-ray crystal structure of the NRP1 b1-VEGF-A fusion protein (Figure 3A). The sequence alignment in Figure 3, shows that there is an insertion of D301 in the NRP2 b1, near the region of the binding site. The insertion reduces the size of the binding site as shown in Figure 3B. In addition, D301 clashes with the central E (*-SCKNTDSRCKARQLELNERTCRCDKPRR) of EG00086. The acid groups of the two amino acids repulse each other and this unfavourable interaction between D301 and E might explain the differences in NRP1 and NRP2 affinities for the peptide that was observed in the ITC experiment mentioned above.

EG00086 and EG3287 binding to NRP1 b1.

To examine why EG00086 is more potent than EG3287, molecular dynamics was used to explore the possible binding conformations of both peptides with NRP1 b1. Dynamic studies were carried out using the above peptide-protein complexes. The EG00086 results provided two observations. Firstly, the local conformation of the EG00086 N-terminus remains approximately linear. Secondly, this N-terminal part of EG00086 is often embedded in a shallow pocket on the protein surface (Figure 3D). The pocket is enclosed by residues T299, S302, E304, and R305, as shown in Figure 3D. It is on the opposite side of the protein away from the main binding site. In addition, the sidechain of Lys (underlined) forms two internal H-bonds with the carbonyl (C=O) near the N-terminus as well as the backbone C=O from Cys (underlined), C₇H₁₅-(C=O)SCKNTDSRCKARQLELNERTCRCDKPRR(OH). The internal H-bond organization (Figure 3E) locks the peptide in a low energy conformation as well as positioning the linear alkyl chain (C₇H₁₅) into the shallow pocket. Conversely, EG3287, which does not have a long N-terminus as does EG00086, is unable to make any interactions with this pocket as shown in Figure 3E. The hydrophobic interaction between the linear alkyl chain of EG00086 and the shallow pocket could explain its slightly better activity with NRP1 b1. We also investigated the conformational stability of EG00086 versus EG3287 through circular dichroism spectra, (Supplementary Figure S1) but no significant difference was noted.

Biological stability of EG00086 and comparison with EG3287.

In order to investigate the suitability of EG00086 for in vitro and in vivo studies we determined the stability of the peptide in cell media and plasma using LCMSMS as a detection method. Both EG3287 and EG00086 were stable in cell media over the duration period of the experiment. In plasma however both peptides exhibited a short half-life of around five minutes. The results of LCMSMS analysis pointed to a cleavage of the C-terminal arginine leading to a more stable metabolite (peptide 9, supplemental figure S2A) that showed little degradation out to 24 h incubation (not shown). An in vivo pharmacokinetic experiment was conducted with the truncated form of EG00086 (peptide 10). This peptide showed relatively short duration and high clearance but was detectable 30 minutes post-dose in mice (Supplemental Figure S2B). Thus the most fragile metabolic site in these

peptides appears to be the terminal arginine and the truncated form retains appreciable activity with increased stability at least in vitro. Further stabilization of the structure will be necessary for long term in vivo experiments.

Binding of EG00086 to tumour cells and its effect on cell viability and response to chemotherapeutic drugs.

EG00086 was next tested for its ability to compete VEGF-A binding to lung A549 and kidney ACHN tumour cells. The peptide potently reduced the specific binding of ¹²⁵I-VEGF-A₁₆₅ to A549 and ACHN cells with the same IC₅₀ of 1 μM (Figure 4A, B). The potency of the peptide in tumour cells was also very similar to that in PAE cells solely expressing NRP1 (Table 1 and Figure 1A). Though A549 and ACHN cells both express NRP1 and NRP2, it is likely that the results in Figure 5 reflect EG00086 inhibition of ¹²⁵I-VEGF-A₁₆₅ binding mainly to NRP1 since ¹²⁵I-VEGF-A₁₆₅ binds to cells expressing NRP2 alone with much lower affinity.^[47] The effects of EG00086 on tumour cell viability were investigated next. Treatment of A549 cells with EG00086 caused a reduction in cell viability, and combined treatment of EG00086 with the cytotoxic chemotherapeutic agents, 5-fluorouracil (5-FU) or paclitaxel, showed enhanced cytotoxicity (IC₅₀ = 4 μM or 55 nM, respectively) than 5-FU alone (IC₅₀ = 47 μM) or paclitaxel alone (IC₅₀ = 199 nM, Figure 4C). In ACHN cells, the peptide also enhanced the cytotoxic potency of paclitaxel, with a reduction in IC₅₀ from 216 nM to 66 nM (Figure 4D). The enhancement of 5-FU and paclitaxel cytotoxicity in the presence of EG00086 is consistent with our previous data showing similar effects of a small molecule antagonist of VEGF-A binding to NRP1, EG00229. However, we do not preclude additional NRP2-mediated effects of the peptides. NRP2-dependent survival has been reported in CNDT 2.5 gastrointestinal cells in which NRP2 knockdown increased sensitivity to 5-FU through a process involving activation of caspases 3 and 7, PARP cleavage and Bcl-2 downregulation.^[48]

Inhibition of tyrosine phosphorylation of p130Cas with EG00086.

Our previous work has identified an important role of NRP1 in mediating VEGF-A and PDGF signalling via p130Cas,^[17-18] an adapter molecule that localises to focal adhesions, and plays an important role in cell migration in endothelial, tumour and other cell types.^[19] Therefore, we investigated the effect of EG00086 on p130Cas tyrosine phosphorylation induced by VEGF-A in human umbilical endothelial cells (HUVECs). VEGF-A (25 ng/mL) stimulated a significant increase in p130Cas tyrosine phosphorylation at 10 minutes, which was inhibited by EG00086 treatment at 100 μM (Figure 5).

Reduction in tumour cell matrix adhesion by EG00086.

The adhesion of cancer cells to the extracellular matrix is an important factor controlling their migration and eventual metastasis. We examined the effect of EG00086 on the adhesion of ACHN cells to five matrices: basement membrane protein complex (BMC), laminin, collagen IV, fibronectin and vitronectin. In all cases EG00086 showed a dose dependent effect (Figure 6A) demonstrating inhibition of adhesion. Comparison of the effect of EG00086 with that of EG3287 showed that EG00086 was more effective than EG3287 in reducing ACHN cell adhesion (Figure 6B).

Conclusions

A series of N-terminal modifications of a peptide corresponding to the C-terminal 28 amino acids of VEGF-A (EG3287) peptide was designed. We observed that an octanoic acid acylation produced the most active peptide, EG00086 with a K_d of 76 nM for NRP1 as determined by SPR. The dissociation off-rate was markedly reduced for this peptide when compared to VEGF-A. Investigation of the thermodynamics of EG00086 binding to NRP1 by ITC showed it to be dominated by enthalpic contributions indicating a high dependency on H-bonding and coulombic effects. Probing this interaction using MD and modeling did not reveal any large interaction of the alkyl chain with the protein, consistent with the ITC result. Disruption of a salt bridge observed in the protein complex of VEGF-NRP1 had a detrimental effect on binding. Two new internal H-bonds observable in the MD studies may give additional stabilization to the peptide and explain the increased activity. The peptide was notably selective for NRP1 with no binding observed to the structurally unrelated protein VEGFR2 and, more surprisingly, three-fold selective over the closely related NRP2 protein. The functional effects of this peptide were correspondingly more potent than those observed with EG3287 and allowed us to demonstrate a range of responses from inhibition of p130Cas phosphorylation and blockade of cell adhesion to an enhancement of the tumoricidal effects of cytotoxic drugs.

One of the most striking observations herein was the inhibition of renal tumour (ACHN) cell adhesion to the ECM proteins, BMC, laminin-I, collagen-IV, and fibronectin matrix by EG00086. These results are particularly relevant in the light of studies indicating an important role of NRP1 in migration and adhesion of several cell types including endothelial and tumour cells.^[18, 22, 47]

Since the integrin β 1-subunit mediates specific cell binding to laminin, collagen, and fibronectin, and has been shown to be a major integrin receptor expressed in carcinoma cells, it is possible that NRP1 cooperates with integrin β 1 in regulation of cell adhesion. Indeed we previously reported a role for NRP1 in integrin β 1 adhesion and our results here support a more potent effect than treatment with the simple, non-acylated bicyclic peptide EG3287.^[38] The role of NRP1 in mediating tumour cell adhesion suggests a potential role for this molecule in metastatic spread. While direct evidence for a role of NRP1 in tumour metastasis is so far lacking, NRP2, expressed in the lymphatics has implicated lymphangiogenesis-mediated tumour metastasis.^[49] The finding that EG00086 inhibits ACHN adhesion to matrix suggests that it and other inhibitors of VEGF-A binding to NRP1 should be examined in models of metastatic tumour spread.

A mechanism through which NRP1 could mediate cell adhesion is by enhancement of signalling pathways relayed via components of focal adhesions, which are thought to play key roles in cell adhesion to extracellular matrix and in integrin signalling.

The finding presented here that EG00086 inhibits VEGF-A induced p130Cas tyrosine phosphorylation provides further evidence that NRP1 is an important mediator of p130Cas signalling, and suggests that inhibition of p130Cas tyrosine phosphorylation is one of the mechanisms underlying the anti-adhesion effect of this peptide observed in ACHN cells. Given the important role of a NRP1/p130Cas pathway in endothelial cell migration it is likely that this pathway is also key mediator of VEGF-A dependent angiogenesis.

Increasing evidence indicates that NRP1 is a new therapeutic target in several cancers. Thus, NRP1 is implicated with VEGF-R2 in the generation of tumour stem cells.^[25] Other studies indicate that NRP1 is highly expressed on some subsets of regulatory T-cells important for suppressing anti-tumour T-cell immunity.^[27] Recent work shows that CendR peptides bind preferentially to NRP1 and thereby promote permeability in tumours and allow better access and effectiveness of therapeutics.^[30] CendR peptides are cyclic and incorporate an RGD type integrin binding motif which is cleaved in vivo to produce a peptide with a terminal arginine that binds NRP1.

One interesting feature is that we were able to demonstrate NRP2 binding for EG00086 with the use of ITC. Although this binding is at least three fold weaker than that observed for NRP1 it indicates that studies utilizing EG00086 must allow for possible NRP2 effects in their interpretation. Our modeling studies clearly indicated a potential clash in the interaction of EG00086 and the D301 of NRP2, perhaps accounting for the reduced affinity compared to NRP1. We observed little change in binding when the penultimate arginine was changed to an alanine residue, despite this being implicated in a structurally important intramolecular salt bridge. We probed the stability of EG00086 in plasma and observed a rapid cleavage of the terminal arginine to a more stable truncated form that also had an R terminus and still maintained significant binding activity. Surprisingly this C-terminal cleavage of arginine has not been reported for VEGF-A even though it might be an expected cleavage site for plasmin. This investigation indicates that potent and effective peptide tools for neuropilin-1 can be assembled. EG00086 has been utilized by us as a standard in dozens of assays and it replaced the non-acylated peptide EG3287 in our systems. Further development of more stable analogues will be required for therapeutic application.

Supplementary data

Detailed chemistry experimental methods can be found with this article online at.....

ACKNOWLEDGEMENTS

Financial support was generously provided by Ark Therapeutics Ltd. We thank Asvi A Francois and Meng-Lin Tsai for technical assistance on ITC. The authors declare no financial interest.

Legend for Table 1

i) Acylation HOBt, DIC, RCO₂H, DMF; ii) Cleavage from resin, 95% TFA, 2.5% EDT, 1.25% TIPS, 1.25% H₂O; iii) First ring formation, K₃Fe(CN)₆, buffer, 50% AcOH; iv) Second ring formation, I₂, TFA/H₂O (v) LC-MS purification

Figure legends

Scheme 1. Synthetic route for the synthesis of bicyclic N-acylated peptides. i) HOBt, DIC, RCO₂H; ii) 95% TFA, 2.5% EDT, 1.25% TIPS, 1.25% H₂O; iii) Fe(CN)₆, buffer, 50% AcOH; iv) A. I₂, TFA/H₂O B. LCMS purification.

Figure 1. Binding of EG00086 to NRP1. Panel A. Specific inhibition of ¹²⁵I-VEGF-A₁₆₅ binding to PAE/NRP1 cells. The N-terminal octanoyl-capped peptide, EG00086, selectively competed with ¹²⁵I-VEGF-A₁₆₅ for binding to PAE cells expressing NRP1 with an IC₅₀ of 1 μM, but had no effect on ¹²⁵I-VEGF-A₁₆₅ binding to PAE/VEGFR-2 cells (panel B). Panel C, SPR sensorgrams of VEGF-A and EG00086 binding to immobilized NRP1. Experimental data (coloured lines) were fit (black lines) with the 1:1 Langmuir binding model for the determination of kinetic constants. The peptide shows potent binding with slower kinetics than VEGF-A.

Figure 2. ITC analysis of EG00086 binding to NRP1 and NRP2. Plots of A, 10 μM NRP2 b1 or B, 5 μM NRP1 b1 in the reaction cell was titrated with the 10-fold higher concentrations of the ligand. **Figure 3.** Modelling of EG00086 into the binding site of NRP1. (A, carbon atom and surface in cyan) and hNRP2 (B and C, carbon atom and surface in green). Partial sequence alignment between the 2 proteins is shown, with insertion D301 from hNRP2 highlighted. For EG00086, only two residues, E and R as bold and italic in the sequence (*-SCKNTDSRCKARQLELNERTCRCDKPRR) are shown for clarity. The carbon atom of EG00086 is shown in orange. A, EG00086 binds to binding site, without any clashes. B, the sidechain of D301 in hNRP2 reduces the size of the binding site. In addition, D301 clashes with E in EG00086 as highlighted in the box in C. D, Modelled EG00086 (carbon atoms in green), showing the possibility of the N-terminus C7 carbon chain (shown in green surface) bound to the shallow pocket. The shallow pocket is enclosed by residues T299, S302, E304, and R305 (labelled and shown in blue). S302 is directly below the peptide. R (bold) in (*-SCKNTDSRCKARQLELNERTCRCDKPRR) binds to the deep pocket on the other side of the protein. E, Overlay of Part of EG00086 (carbon atoms in green) and EG3287 (carbon atoms in cyan). In the EG00086-NRP1 docked complex, the sidechain of Lys frequently formed two internal H-bonds (in dashed lines) with the C=O near the N-terminus as well as the backbone C=O of Cys. In the EG3287-NRP1 complex, EG3287, without the long N-terminus cannot reach the shallow pocket.










Figure 4. Bind of EG00086 to tumour cells and potentiation of cytotoxicity of standard cytotoxics. A EG00086 shows specific inhibition of ¹²⁵I-VEGF-A₁₆₅ binding to A549 and B. ACHN cells. C Treatment of A549 cells with the peptide caused a reduction in cell viability, and combined treatment of EG00086 and 5-fluouracil (5-FU) or paclitaxel showed more effective cytotoxicity (IC₅₀ = 4 μM or 55 nM than 5-FU alone (IC₅₀ = 47 μM) or palitaxel alone (IC₅₀ =199 nM). In ACHN cells, the peptide also enhanced the cytotoxic potency of paclitaxel (panel D).

Figure 5: VEGF-A stimulated tyrosine phosphorylation of p130Cas is dependent on the ability of VEGF-A to bind NRP1. (A), HUVECs were grown to confluence and shifted to medium containing 0.5% serum for 16 h. Cells were pre-incubated for 30 min with 2, 20 & 100 μM EG00086, vehicle (control) followed by stimulation with 25ng/ml VEGF-A (V) or with no further treatment (control, C) for 10 min. Cell lysates were then prepared, blotted, and probed with the indicated antibodies. Blots shown here are representative of at least four separate experiments. Quantitation of p130Cas phosphorylation was performed by

densitometry using Image J. Data are presented as p130Cas phosphorylation relative units (RU) (means +/- s.e.m.) normalized to total p130Cas; $p < 0.05 = *$

Figure 6: Blockade of cancer cell adhesion with EG00086. A. EG00086 treatment decreased adhesion of kidney carcinoma ACHN cells (expressing NRP1/NRP2) to extracellular matrix proteins in a dose-dependent manner. B. EG00086 is more effective at reducing adhesion of ACHN cells to matrix proteins than EG3287.

Table 1. Structures and NRP1 binding affinities in NRP1-expressing PAE cells.

ID	Structure	% binding at 100 μ M	IC ₅₀ (μ M)
1, EG3287			4.1 \pm 0.05
2, EG00086 a			1.2 \pm 0.09
3 ^a			2.3 \pm 0.15
4 ^a		>70	
5 ^a		>70	
6 ^a		>70	
7 ^b			2.2 \pm 0.10
8 ^b		66	
9 ^c			6.4 \pm 0.05

10^d7.3
±0.01

^aN-acylated, ^bN-acylated DKPAR-OH change, ^ctruncated, ^dN-acylated truncated.

Table 2. Thermodynamics of EG00086 binding to NRP1 and NRP2 protein as determined by ITC

Protein	Kd (μM)	ΔH (Cal/mol)	ΔS (Cal/mol)	N
NRP2b1	3.64 ±1.17	-2472 ±584	16.5	0.95 ±0.15
NRP2b1 (15 °C)	2.87 ±0.26	-6212 ±320	3.43	0.92 ±0.035
NRP1b1	0.88 ±0.16	-9405 ±1290	-4.24	0.89 ±0.084

References

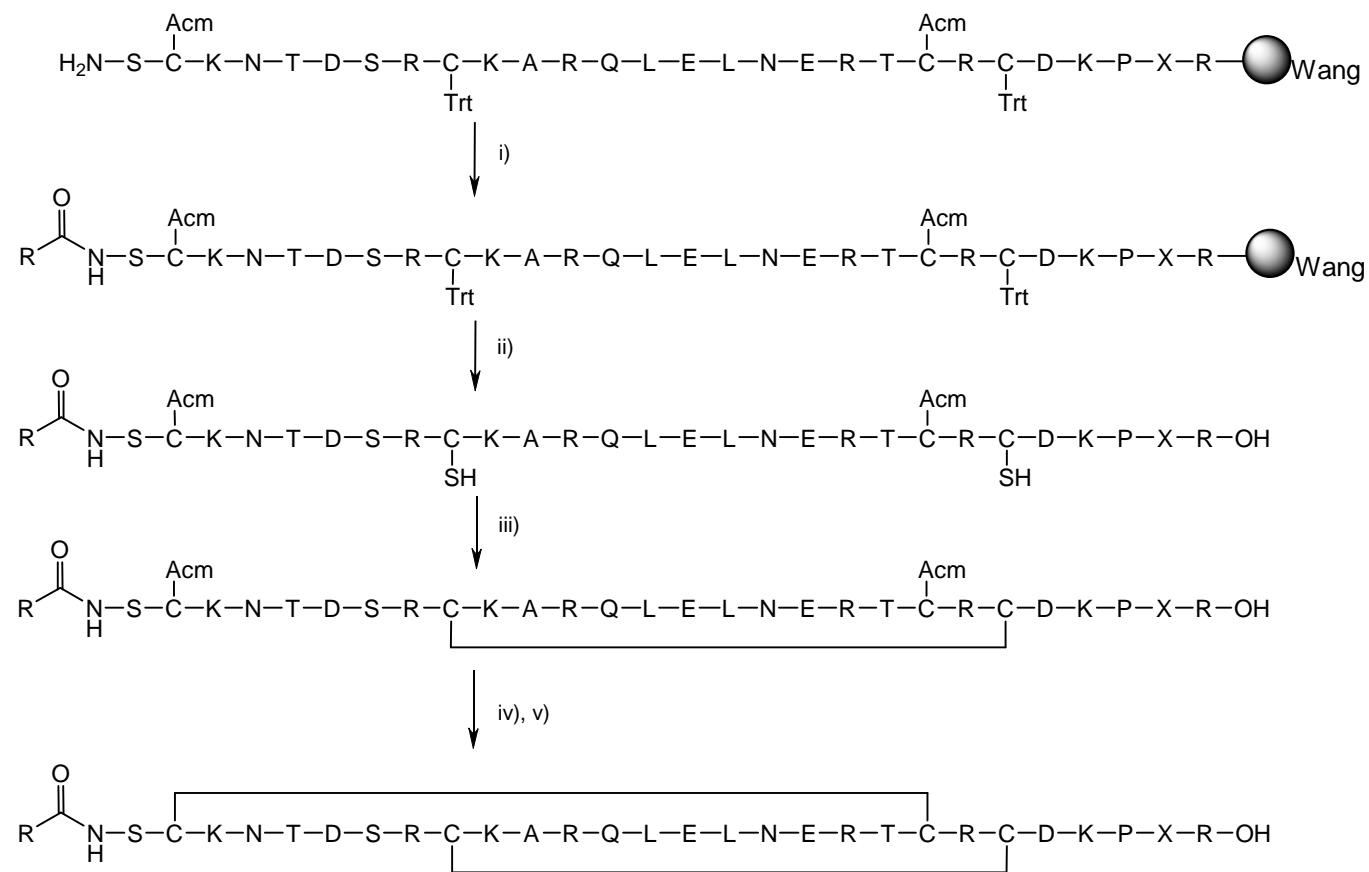
- [1] C. Raimondi, C. Ruhrberg, *Semin. Cell Dev. Biol.* **2013**, *24*, 172-178.
- [2] M. W. Parker, H. F. Guo, X. Li, A. D. Linkugel, C. W. Vander Kooi, *Biochemistry* **2012**, *51*, 9437-9446.
- [3] A. Lanahan, X. Zhang, A. Fantin, Z. Zhuang, F. Rivera-Molina, K. Speichinger, C. Prahst, J. Zhang, Y. Wang, G. Davis, D. Toomre, C. Ruhrberg, M. Simons, *Dev. Cell* **2013**, *25*, 156-168.
- [4] M. Rossignol, M. L. Gagnon, M. Klagsbrun, *Genomics* **2000**, *70*, 211-222.
- [5] H. Fujisawa, T. Kitsukawa, *Curr. Opin. Neurobiol.* **1998**, *8*, 587-592.
- [6] S. Djordjevic, P. C. Driscoll, *Drug discovery today* **2013**, *18*, 447-455.
- [7] T. Kitsukawa, M. Shimizu, M. Sanbo, T. Hirata, M. Taniguchi, Y. Bekku, T. Yagi, H. Fujisawa, *Neuron* **1997**, *19*, 995-1005.
- [8] T. Kawasaki, T. Kitsukawa, Y. Bekku, Y. Matsuda, M. Sanbo, T. Yagi, H. Fujisawa, *Development (Cambridge, England)* **1999**, *126*, 4895-4902.

- [9] A. L. Kolodkin, D. V. Levengood, E. G. Rowe, Y. T. Tai, R. J. Giger, D. D. Ginty, *Cell* **1997**, *90*, 753-762.
- [10] Z. He, M. Tessier-Lavigne, *Cell* **1997**, *90*, 739-751.
- [11] S. Soker, S. Takashima, H. Q. Miao, G. Neufeld, M. Klagsbrun, *Cell* **1998**, *92*, 735-745.
- [12] C. Gu, B. J. Limberg, G. B. Whitaker, B. Perman, D. J. Leahy, J. S. Rosenbaum, D. D. Ginty, A. L. Kolodkin, *J. Biol. Chem.* **2002**, *277*, 18069-18076.
- [13] P. Frankel, C. Pellet-Many, P. Lehtolainen, G. M. D'Abaco, M. L. Tickner, L. Cheng, I. C. Zachary, *EMBO reports* **2008**, *9*, 983-989.
- [14] Y. Glinka, G. J. Prud'homme, *J. Leukocyte Biol.* **2008**, *84*, 302-310.
- [15] I. M. Evans, G. Britton, I. C. Zachary, *Cell. Signalling* **2008**, *20*, 1375-1384.
- [16] P. Di Stefano, M. P. Leal, G. Tornillo, B. Bisaro, D. Repetto, A. Pincini, E. Santopietro, N. Sharma, E. Turco, S. Cabodi, P. Defilippi, *Am. J. Cancer Res.* **2011**, *1*, 663-673.
- [17] C. Pellet-Many, P. Frankel, I. M. Evans, B. Herzog, M. Junemann-Ramirez, I. C. Zachary, *Biochem. J.* **2011**, *435*, 609-618.
- [18] I. M. Evans, M. Yamaji, G. Britton, C. Pellet-Many, C. Lockie, I. C. Zachary, P. Frankel, *Mol. Cell. Biol.* **2011**, *31*, 1174-1185.
- [19] A. Barrett, C. Pellet-Many, I. C. Zachary, I. M. Evans, P. Frankel, *Cell. Signalling* **2013**, *25*, 766-777.
- [20] Y. Wang, M. A. McNiven, *J. Cell Biol.* **2012**, *196*, 375-385.
- [21] S. Niland, B. Ditkowski, D. Parrandier, L. Roth, H. Augustin, J. A. Eble, *Arterioscler., Thromb., Vasc. Biol.* **2013**, *33*, 544-554.
- [22] Q. Pan, Y. Chanthery, W. C. Liang, S. Stawicki, J. Mak, N. Rathore, R. K. Tong, J. Kowalski, S. F. Yee, G. Pacheco, S. Ross, Z. Cheng, J. Le Couter, G. Plowman, F. Peale, A. W. Koch, Y. Wu, A. Bagri, M. Tessier-Lavigne, R. J. Watts, *Cancer cell* **2007**, *11*, 53-67.
- [23] M. Caunt, J. Mak, W. C. Liang, S. Stawicki, Q. Pan, R. K. Tong, J. Kowalski, C. Ho, H. B. Reslan, J. Ross, L. Berry, I. Kasman, C. Zlot, Z. Cheng, J. Le Couter, E. H. Filvaroff, G. Plowman, F. Peale, D. French, R. Carano, A. W. Koch, Y. Wu, R. J. Watts, M. Tessier-Lavigne, A. Bagri, *Cancer cell* **2008**, *13*, 331-342.
- [24] B. Beck, G. Driessens, S. Goossens, K. K. Youssef, A. Kuchnio, A. Caauwe, P. A. Sotiropoulou, S. Loges, G. Lapouge, A. Candi, G. Mascré, B. Drogat, S. Dekoninck, J. J. Haigh, P. Carmeliet, C. Blanpain, *Nature* **2011**, *478*, 399-403.
- [25] P. Hamerlik, J. D. Lathia, R. Rasmussen, Q. Wu, J. Bartkova, M. Lee, P. Moudry, J. Bartek, Jr., W. Fischer, J. Lukas, J. N. Rich, J. Bartek, *J. Exp. Med.* **2012**, *209*, 507-520.
- [26] M. Yadav, C. Louvet, D. Davini, J. M. Gardner, M. Martinez-Llordella, S. Bailey-Bucktrout, B. A. Anthony, F. M. Sverdrup, R. Head, D. J. Kuster, P. Ruminski, D. Weiss, D. Von Schack, J. A. Bluestone, *J. Exp. Med.* **2012**, *209*, 1713-1722.
- [27] W. Hansen, *Oncoimmunology* **2013**, *2*, e23039.
- [28] H. Jia, A. Bagherzadeh, B. Hartzoulakis, A. Jarvis, M. Lohr, S. Shaikh, R. Aqil, L. Cheng, M. Tickner, D. Esposito, R. Harris, P. C. Driscoll, D. L. Selwood, I. C. Zachary, *J. Biol. Chem.* **2006**, *281*, 13493-13502.
- [29] A. Starzec, P. Ladam, R. Vassy, S. Badache, N. Bouchemal, A. Navaza, C. H. du Penhoat, G. Y. Perret, *Peptides* **2007**, *28*, 2397-2402.
- [30] T. Teesalu, K. N. Sugahara, V. R. Kotamraju, E. Ruoslahti, *Proc. Natl. Acad. Sci. U. S. A.* **2009**, *106*, 16157-16162.
- [31] J. A. Getz, O. Cheneval, D. J. Craik, P. S. Daugherty, *ACS Chem. Biol.* **2013**.
- [32] B. A. Appleton, P. Wu, J. Maloney, J. Yin, W. C. Liang, S. Stawicki, K. Mortara, K. K. Bowman, J. M. Elliott, W. Desmarais, J. F. Bazan, A. Bagri, M. Tessier-Lavigne, A. W. Koch, Y. Wu, R. J. Watts, C. Wiesmann, *EMBO J.* **2007**, *26*, 4902-4912.
- [33] A. Jarvis, C. K. Allerston, H. Jia, B. Herzog, A. Garza-Garcia, N. Winfield, K. Ellard, R. Aqil, R. Lynch, C. Chapman, B. Hartzoulakis, J. Nally, M. Stewart, L. Cheng, M. Menon, M. Tickner, S. Djordjevic, P. C. Driscoll, I. Zachary, D. L. Selwood, *J. Med. Chem* **2010**, *53*, 2215-2226.

- [34] S. M. Alam, C. A. Paleos, H. X. Liao, R. Scarce, J. Robinson, B. F. Haynes, *AIDS Res. Hum. Retroviruses* **2004**, *20*, 836-845.
- [35] R. C. Bravo Gonzalez, J. Huwyler, I. Walter, R. Mountfield, B. Bittner, *Int. J. Pharmaceutics* **2002**, *245*, 143-151.
- [36] L. Li, T. A. Leedom, J. Do, H. Huang, J. Lai, K. Johnson, T. F. Osothprarop, J. D. Rizzo, V. R. Doppalapudi, C. W. Bradshaw, R. W. Lappe, G. Woodnutt, N. J. Levin, S. R. Pirie-Shepherd, *Translational Oncology* **2011**, *4*, 249-257.
- [37] L. Cheng, H. Jia, M. Lohr, A. Bagherzadeh, D. I. Holmes, D. Selwood, I. Zachary, *J. Biol. Chem.* **2004**, *279*, 30654-30661.
- [38] H. Jia, L. Cheng, M. Tickner, A. Bagherzadeh, D. Selwood, I. Zachary, *Br J Cancer* **2010**, *102*, 541-552.
- [39] L. H. Brinckerhoff, V. V. Kalashnikov, L. W. Thompson, G. V. Yamshchikov, R. A. Pierce, H. S. Galavotti, V. H. Engelhard, C. L. Slingluff, Jr., *Int. J. Cancer* **1999**, *83*, 326-334.
- [40] J. R. Holder, F. F. Marques, Z. Xiang, R. M. Bauzo, C. Haskell-Luevano, *Eur. J. Pharmacol.* **2003**, *462*, 41-52.
- [41] A. Seyedarabi, L. Cheng, I. Zachary, S. Djordjevic, *PLoS One* **2013**, *8*, e55690.
- [42] M. W. Parker, P. Xu, X. Li, C. W. Vander Kooi, *J. Biol. Chem.* **2012**, *287*, 11082-11089.
- [43] C. W. Vander Kooi, M. A. Jusino, B. Perman, D. B. Neau, H. D. Bellamy, D. J. Leahy, *Proc. Natl. Acad. Sci. U. S. A.* **2007**, *104*, 6152-6157.
- [44] R. Karlsson, H. Roos, L. Fägerstam, B. Persson, *Methods* **1994**, *6*, 99-110.
- [45] G. Fuh, K. C. Garcia, A. M. de Vos, *J. Biol. Chem.* **2000**, *275*, 26690-26695.
- [46] M. O. E. MOE, 10 ed., Chemical Computing Group, **2011**.
- [47] B. Herzog, C. Pellet-Many, G. Britton, B. Hartzoulakis, I. C. Zachary, *Mol. Biol. Cell* **2011**, *22*, 2766-2776.
- [48] S. Samuel, P. Gaur, F. Fan, L. Xia, M. J. Gray, N. A. Dallas, D. Bose, C. Rodriguez-Aguayo, G. Lopez-Berestein, G. Plowman, A. Bagri, A. K. Sood, L. M. Ellis, *PLoS ONE* **2011**, *6*, e23208.
- [49] Y. Xu, L. Yuan, J. Mak, L. Pardanaud, M. Caunt, I. Kasman, B. Larrivee, R. Del Toro, S. Suchting, A. Medvinsky, J. Silva, J. Yang, J. L. Thomas, A. W. Koch, K. Alitalo, A. Eichmann, A. Bagri, *J Cell Biol* **2010**, *188*, 115-130.

Figures

Scheme 1.



For definitions of R and X see Table 1

 = Wang [p-alkoxybenzyl alcohol] linker

Trt = triphenylmethyl; Acm = acetamidomethyl

Figure 1

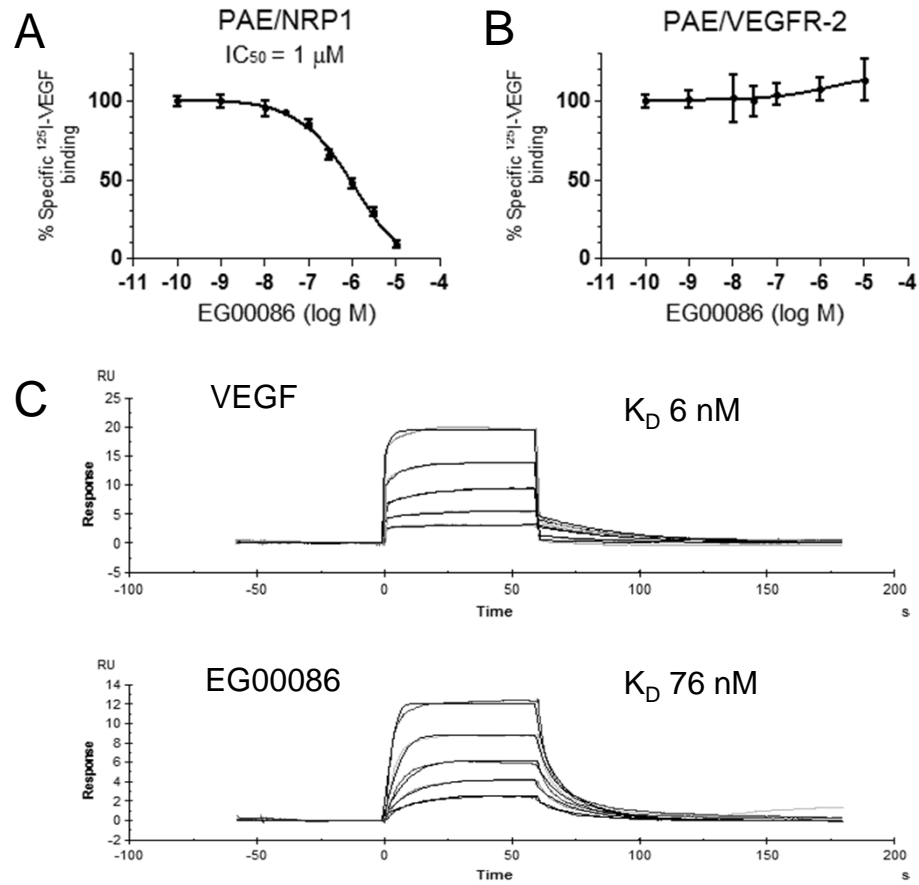


Figure 2

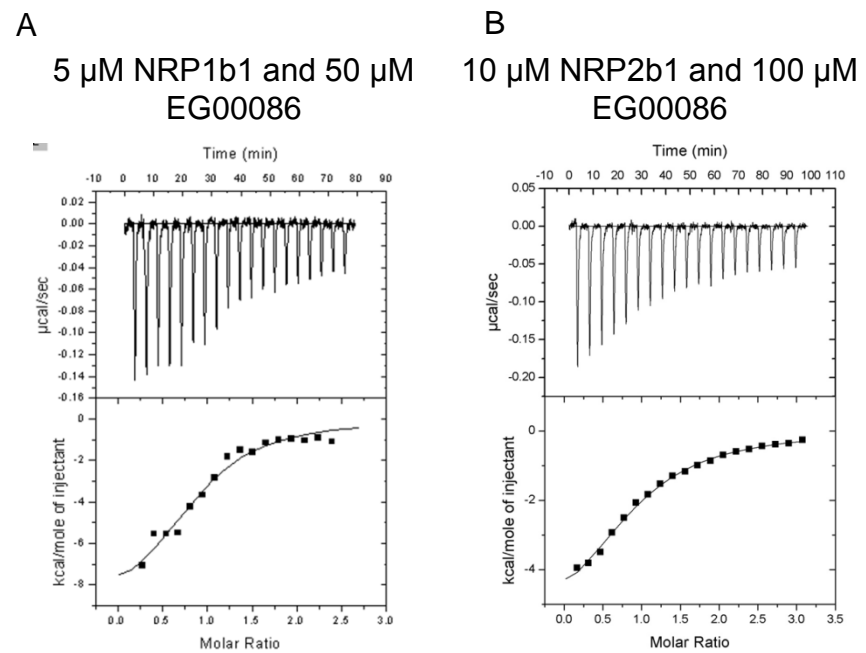


Figure 3

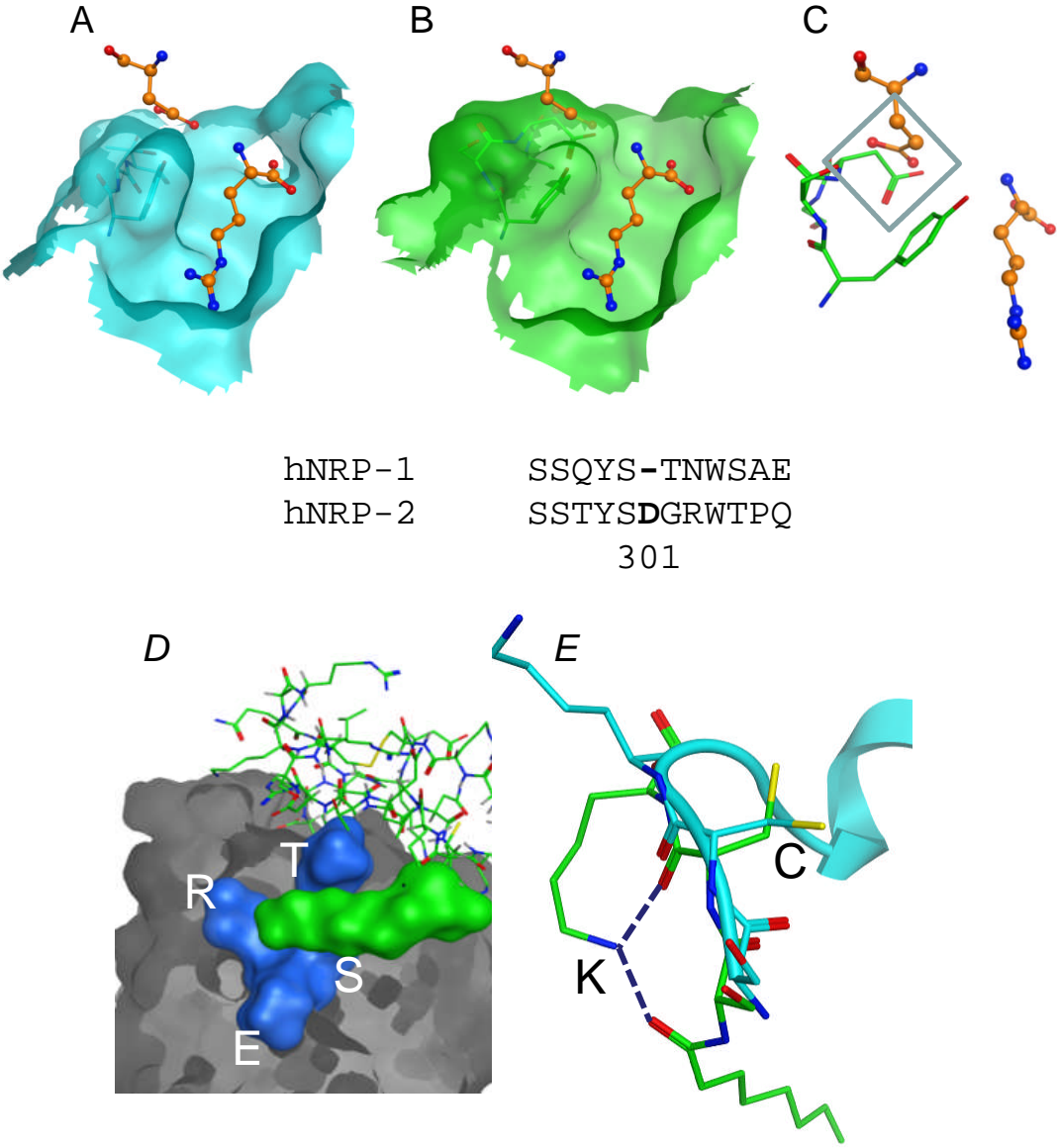


Figure 4.

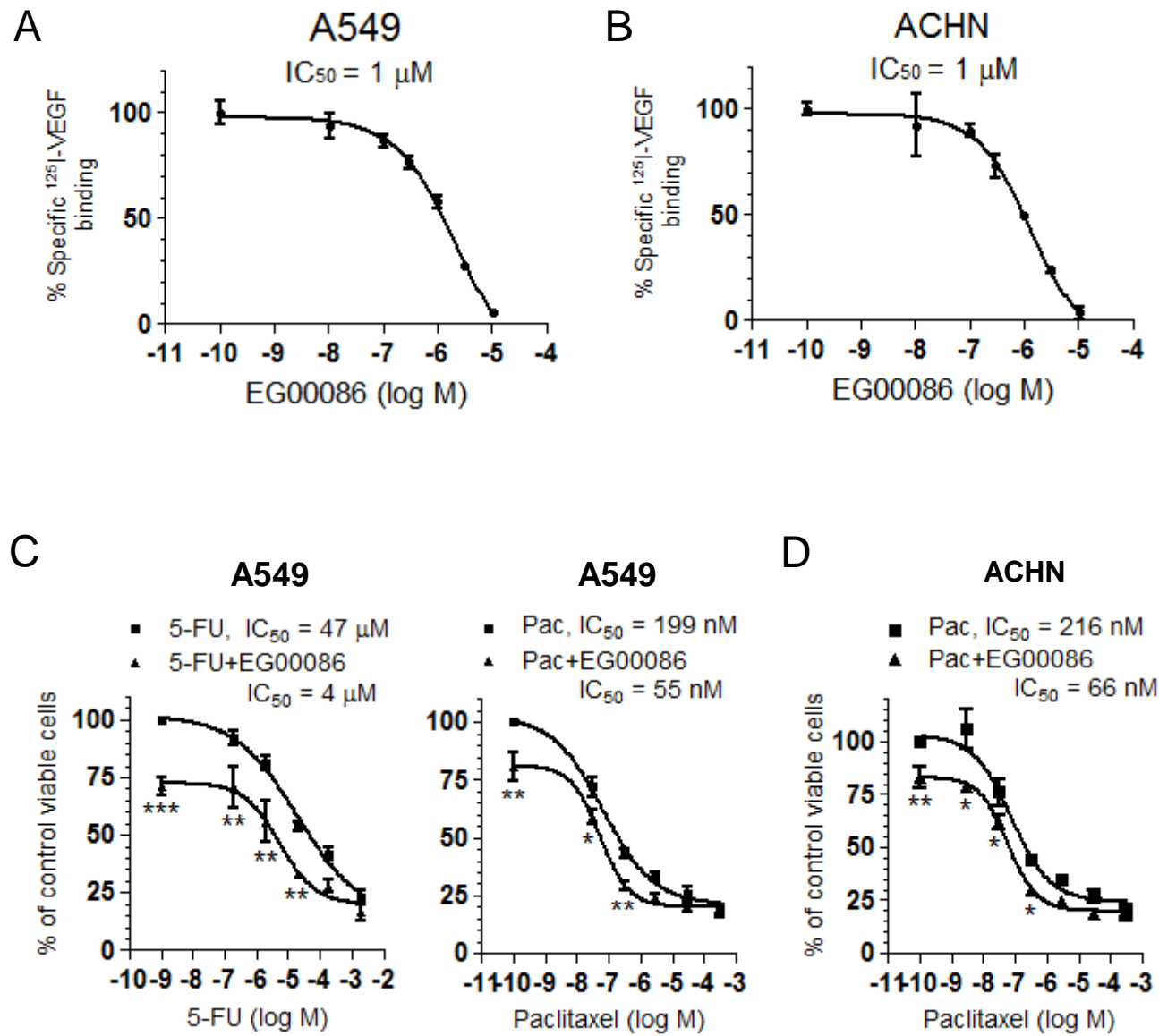


Figure 5

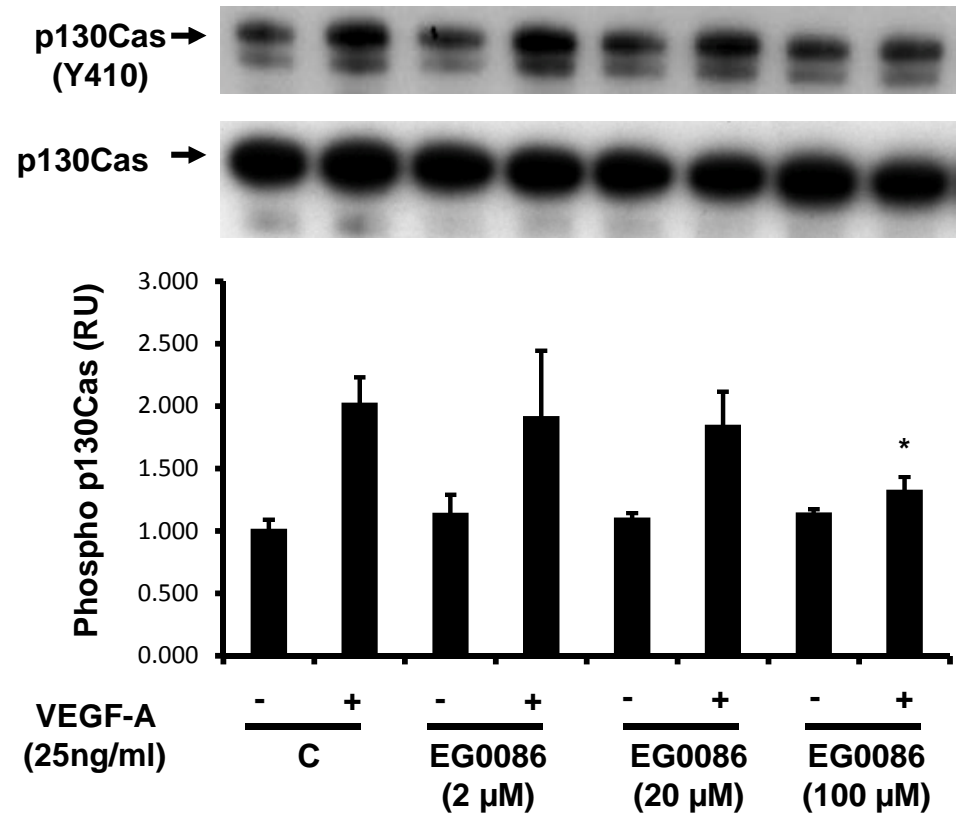


Figure 6

